Received: 24 March 2021 | Revised: 2 June 2021 | Accepted: 2 July 2021

DOI: 10.1002/pat.5450

RESEARCH ARTICLE

polymers advanced technologies WILEY

Influence of the hydrophilicity of montmorillonite on structure and properties of thermoplastic wheat starch/montmorillonite bionanocomposites

Irene Derungs[1] | Maite Rico[1] | Joaquín López[1] | Luis Barral[1,2] | Belén Montero[1] | Rebeca Bouza[1]

[1]Grupo de Polímeros, Departamento de Física y Ciencias de la Tierra, Universidade da Coruña, Escuela Universitaria Politécnica, Ferrol, Spain

[2]Cellular and Molecular Cardiology Research Unit. Institute of Biomedical Research (IDIS-SERGAS), University Clinical Hospital, Santiago de Compostela, Spain

Correspondence
Maite Rico, Grupo de Polímeros, Departamento de Física y Ciencias de la Tierra, Universidade da Coruña, Escuela Universitaria Politécnica, Serantes, Avda. 19 de Febrero s/n, Ferrol 15471, Spain.
Email: maite.rico@udc.es

Funding information
FEDER, Grant/Award Number: ED-431C 2019/17; Xunta de Galicia Government; Funding for open access charge: Universidade da Coruña/CISUG

Abstract

The increasing environmental pollution with petroleum-based plastics has advanced research on biodegradable polymers. Thermoplastic starch (TPS) is one promising candidate due to wide availability from various renewable sources, low cost and biodegradability. However, TPS has significant shortcomings, as high water sensitivity and low mechanical properties. An approach to overcome these drawbacks is adding nanofillers as reinforcement of the starch matrix. Among the nanofillers, montmorillonite clays have the advantages of a wide availability, low cost, versatility and environmental friendliness. Bionanocomposites based on wheat starch plasticized with glycerol and reinforced with three types of montmorillonite nanoclays, one natural (Cloisite Na^+) and two organomodified (Cloisite 30B and Cloisite 10A), were prepared by melt processing. The effect of nanoclay type and amount on processing properties, thermal stability, dynamic mechanical properties and water absorption was widely investigated. The properties strongly depended on the dispersion state of the nanoclay in the TPS matrix. The dispersion improved with the hydrophilicity of the nanoclay. Cloisite Na^+, the most hydrophilic nanoclay, was the most effective in reinforcing TPS, improving the thermal stability and the dynamic mechanical properties, and showing a greater resistance to water absorption in normal humidity environments. Bionanocomposites of TPS andCloisite Na^+ can be a good alternative for use in packaging applications.

KEYWORDS
bionanocomposites, montmorillonite clay, thermoplastic starch

1 | INTRODUCTION

As a result of the increasing environmental concerns and the shortage of fossil resources, the last decade has seen the development of efficient solutions to produce new environmentally friendly materials. Biopolymers, biodegradable and produced from renewable sources, are an innovating answer to replace conventional petroleum-based plastics.[1] Among these biopolymers, starch is considered as one of the most promising materials due to its advantages such as low cost, wide availability, total compostability without toxic residues and renewable origin. Starch is not a thermoplastic in its native form, however, in the presence of a suitable plasticizer, temperature, and shear, the starch granules can be converted into thermoplastic starch (TPS), which can be processed as conventional thermoplastics.[2–4] In spite of its

benefits, TPS still has significant disadvantages that limits its use in industrial applications, that is, high moisture sensitivity and low mechanical properties, which also vary with time and humidity.

The incorporation ofdifferent fillers into TPS matrices to produce composite materials can be a solution toreduce these drawbacks and improve the performance of starch-based materials.[5] Compared to conventional composites, nanocomposites obtained by the incorporation of nano-sized fillers into TPS matrices can improve more stronglythe properties even at low nanofiller contents due to the large surface area resulting in the possibility of numerousinteractions between the polymer matrix and the nanofillers.[6,7]

Among the nanofillers, special attention has been given to the layered silicates, known as nanoclays, and especially on montmorillonites (MMT), due to their wide availability, low cost, versatility, environmentally friendly and low toxicity.[8–10] MMT have astacked platelet structurewith a thickness of approximately 1 nanometer and lateral dimensions inthe order of micrometers. MMT is a 2:1 layertype phyllosilicate composed of acentral alumina octahedral sheet sandwiched between two silica tetrahedral sheets. Isomorphic substitutions take place inside these clay platelets which induce a negative charge that is naturally counter balanced by the presence of inorganic cations (Na^+, Ca^{2+}, ...) into the interlayer spacing leading to a hydrophilic character. An ion-exchange reaction of these inorganic cations by different organic surfactants can be carried outresulting in differentorganomodified MMT,[11] which have a higher hydrophobic character and a greater interlayer spacing.

Due to their high surface area and cation exchange, as well as their excellent mechanical properties and thermal resistance, MMT have been an effective filler for differentpolymer matrices, from rubbers[12] to synthetic polymers, such as polystyrene,[13] biopolymers, as polylactide[14] and starch,[15,16] as well as polymer blends.[17,18] It has been reported that the incorporation of a low level of MMT into polymer matrices can significantly improve a large number of physical properties of the virgin polymer, including mechanical and barrier properties, thermal stability, flammability resistance and degradability of biodegradable polymers.[19–21] This improvement in the properties is usually conditioned to a good dispersion of MMT in the polymeric matrix, where the polymeric chains from the bulk penetrate inside the clay layers forming intercalated or exfoliated nanostructures.[22]Therefore, it is expected that the addition of suitable nanoclays to TPS matrices leading to bionanocomposites with good dispersion and strong matrix-clay interaction is an effective approach to improve the properties reducing the drawbacks of starch-based materials.

Despite the studies carried out, a comprehensive and detailed study on the different aspects of the behavior of starch/MMT bionanocomposites depending on the amount and type of MMT and its compatibility with starch is still lacking, as it was thepurpose in this work. Thus, the aim of this work was to develop environmentally friendly bionanocomposites based on wheat starch plasticized with glycerol and reinforced with different MMT nanoclays (TPS/MMT bionanocomposites) for their potential use in packaging applications. Three types of MMT were investigated, one natural (Cloisite Na^+) and two organomodified (Cloisite 30B and Cloisite10A) differentiated in the counter-cation. The effect of nanoclay type and amount on processing properties, thermal stability, dynamic mechanical properties and water absorption at different environmental humidity was analyzed and discussed in detail. The results were related to the dispersion and structure of the different nanoclays in the TPS matrix.

2 | EXPERIMENTAL SECTION

2.1 | Materials

Wheat starch was kindly supplied by Roquette containing 25% amylose according to the manufacturer data. The moisture content was of 12 wt.% determined by gravimetric method. Glycerol supplied by Sigma-Aldrich with a 99.5% purity was used as plasticizer.

As fillers, three types of MMT clays were used from Southern Clay Products: one natural MMT, Cloisite Na^+ (CNa), and two organomodified MMT, Cloisite 30B (C30B) and Cloisite 10A (C10A). The organomodified MMT differ in the ammonium counter-cation nature. Thus, C30B is modified with methyl tallow bis-2-hydroxyethyl quaternary ammonium cations, while C10A is modified with dimethyl benzyl hydrogenated tallow quaternary ammonium cations. Structural characteristics of the nanoclays are shown in Table 1. It is important note that the surface hydrophilicity of nanoclays follows the order CNa> C30B > C10A.

2.2 | Preparation of TPS and TPS/MMT bionanocomposites

TPSs were prepared maintaining the starch/glycerol ratio at 65/35 in all blends. Nanoclays were added in amounts of 1 wt.%, 3 wt.% and 5 wt.%. All amounts were based in dry weight. The samples were coded specifying type and content of nanoclay as shown in Table 2.

Neat TPS and TPS/MMT bionanocomposites were melt processed in an internal mixer (Brabender W50-E, 3 zones PL-type 2000–3, Duisburg, Germany). The plasticization of the starch and the dispersion of the nanoclay were performed in the same processing step. For that, each component of the samples, that is, starch, glycerol plasticizer and MMT nanoclay (in the case of composites), were first premixed manually at room temperature and then introduced into the internal mixer. The processing was carried out at 120°C with a rotor speed of 60 rpm for 15 min. The processed samples were compression-molded by using a hot press (IQAP LAP PL-15, Cataluña, Spain) at 120°C and 100 bar of pressure.

2.3 | Characterization of TPS and TPS/MMT bionanocomposites

2.3.1 | Scanning electron microscopy coupled with energy dispersive X-ray analysis (SEM/EDX)

Mapping of the silicon distributionon fracture surfaces of TPS/MMT bionanocomposites were obtainedusing a scanning electron

TABLE 1 Structural characteristics of the nanoclays

Trade name	Code	Counter-cation	2θ (°)	d_{001} (nm)
Cloisite Na^+	CNa	Na^+	7.15	1.23
Cloisite 30B	C30B	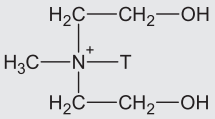	4.78	1.85
Cloisite 10A	C10A	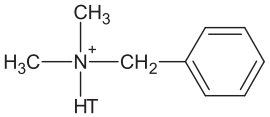	4.57	1.93

Note: T = Tallow; HT = hydrogenated Tallow.
2θ: diffraction peak position from X-ray diffraction (XRD).
d_{001}: interlayer spacing calculated from 2θ value.

TABLE 2 Composition and parameters of processing and XRD data for TPS and TPS/MMT bionanocomposites

Sample	Nanoclay type	Nanoclay (wt. %)	Starch/glycerol 65/35 (wt.%)	Steady torque (Nm)	d_{001} (nm)
TPS	-	0	100	9.6	-
TPS-1CNa	CNa	1	99	10.8	-
TPS-3CNa	CNa	3	97	12.5	1.85
TPS-5CNa	CNa	5	95	14.0	1.85
TPS-1C30B	C30B	1	99	10.7	-
TPS-3C30B	C30B	3	97	11.2	2.00
TPS-5C30B	C30B	5	95	13.3	1.99
TPS-1C10A	C10A	1	99	10.8	-
TPS-3C10A	C10A	3	97	11.8	1.83
TPS-5C10A	C10A	5	95	12.6	1.93

microscope (JEOL-JSM 6400, Tokyo, Japan) operated at 20 kV coupled to an energy dispersive X-ray detector (EDX). Prior to analysis, samples were fractured under liquid nitrogen and coated with a carbon layer.

2.3.2 | X-ray diffraction (XRD)

The interlayer spacing of the clays (d_{001}) was studied by X-ray diffraction (XRD) using a Siemens D5000 diffractometer (Karlsruhe, Germany). The equipment operated at a current of 30 mA and voltage of 40 kV. The wavelength of the copper anode is $\lambda(K_\alpha) = 0.15406$ nm. Scans were performed from $2\theta = 2°$ to 10° at scanning step rate of 0.02° in step time of 4 s. d_{001} was calculated by Equation (1) from the position of the first clay diffraction peakusing the Bragg's law.

$$2d_{001}\sin\theta = \lambda \quad (1)$$

2.3.3 | Thermogravimetric analysis (TGA)

Thermal stability of nanoclays, neat TPS and TPS/MMT bionanocomposites was evaluated using a thermogravimetric analyzer Perkin Elmer TGA 7 (Massachusetts) in a temperature range between 50°C and 600°C at a heating rate of 10°C min^{-1} under inert argon atmosphere.

2.3.4 | Dynamic mechanical analysis (DMA)

Dynamic mechanical properties of materials were determined from a Perkin Elmer DMA7 (Massachusetts) device using a three-point bending geometry. Specimens were cut from molded parts with dimensions of 20 × 5 × 3 mm^3 and tested. DMA curves were recorded as a function of temperature from −70°C to 50°C with a constant heating rate of 5°C min^{-1} and a frequency of 1 Hz.

2.3.5 | Water absorption

Water absorption tests were carried out to all materials under four different relativehumidity (RH) environments (33%, 54%, 75% and 95%). To create these environments, saturated solutions of magnesium chloride hexahydrate ($MgCl_2{\cdot}6H_2O$), magnesium nitrate hexahydrate ($Mg[NO_3]_2{\cdot}6H_2O$), sodium chloride (NaCl) and potassium nitrate (KNO_3) were respectively prepared following the UNE-EN ISO 2006: 483 in hermetic containers conditioned at 20°C ± 2°C.

Samples of each neat TPS and TPS/MMT bionanocomposites were cut with dimensions of 8 × 8 × 3 mm^3, dried at 70°C for 72 h, cooled, and weighed. Immediately after, the samples were placed in the containers with the different RH environments. The samples were periodically weighed in an analytical balance and returned to the containers. The percentage of water absorbed at each time was calculated according to Equation (2).

$$\text{Water absorption}\,(\%) = \frac{M_t - M_0}{M_0} \times 100, \qquad (2)$$

where M_0 is the weight of the dry sample and M_t is the weight at time t.

3 | RESULTS AND DISCUSSION

3.1 | Processing properties

During processing of starch in an internal mixer it is expected that plasticization of starch occurs with the complete or partial destruction of its initial crystalline order resulting in TPS. An efficient dispersion of the nanoclay in the TPS matrix is desired to obtain TPS/MMT bionanocomposites with improved properties. According to Dennis et al.[23] in addition to the polymer/clay affinity, two processing parameters favor the dispersion, that is, high shear and long residence times. High shear induces the delamination of clay platelets from tactoids, and an extended residence time allows the diffusion of the polymer chains into the interlayer spacing. However, these parameters would also contribute to the degradation of starch molecules.[10]

The torque versus time curves during processing were registered for TPS/MMT bionanocomposites and neat TPS (see supplementary material, Figure A1). The torque curves followed a similar trend in all materials, with a rapid initial torque increase to a maximum attributed to the plasticization process, and then the torque gradually decreased until reaching a steady state. Although the steady state was reached in all the samples after about 5 min, a residence time of 15 min was followed to favor the clay dispersion. At that time, the torque values remained practically constant indicating no degradation of starch chain or loss of plasticizer during the materials processing.

The torque values at steady state for TPS/MMT bionanocomposites and neat TPS are summarized in Table 2. Steady torque can be used as a comparative estimation of the viscosity of the melted material under the used processing conditions, which dependson mobility of the starch molecular chains in such conditions.

The incorporation of any of the nanoclaysled to an increase in the steady torque of neat TPS, increasing with higher nanoclay content. It indicates that the viscosity of the meltedmaterial is increased in the TPS/MMT bionanocomposites. Similarbehavior was observed by other authors.[24] An intercalated (non-exfoliated) structure of the bionanocomposites can explain this behavior. In the intercalated structure, a mass of TPS chains is intercalated into the clay platelets increasing the interlayer spacing but remaining tactoids of the clay. Tactoids cannot be oriented by the shear stress, resulting in an increase of viscosity and steady torque. It is contrary to that expected for an exfoliated structure where the clay platelets are almost individually dispersed into the matrix. According to Chivrac et al.[11] in the exfoliated structure, these platelets can easy be oriented by the shear stress and thus the melt viscosity should not increase. They observed this behavior for TPS reinforced with the highly compatible clays modified with cationic starch.

As for the nanoclay type, the addition of 1 wt.% of nanoclay led to similar increases in viscosity for any of the three MMT. However, torque differences were found depending on the nanoclay typeat higher clay amounts, being higher the viscosity with the natural CNa. The better compatibility of starch with the more hydrophilic CNa must lead to stronger interactions of the starch molecular chains with this nanoclay. It would cause a greater restriction to the movement of starch molecular chains, increasing the melt viscosity and explaining the highest torque values for TPS/CNa bionanocomposites.

3.2 | Dispersion state of the nanoclays in the TPS matrix

As stated above, a homogeneous dispersion of nanoclay in the TPS matrix is desired. Transparency of bionanocomposites can be used as an indirect and roughly measure of the dispersion of the nanoclays in the matrix. Composites containing particles that are smaller than the wavelength of visible light are transparent while larger particles or aggregates scatter light making the material opaque.[25] The transparency of TPS/MMT bionanocomposites and neat TPS was examined visually against a background image (see supplementary material, Figure A2).

Bionanocomposites with natural CNa were homogeneous and translucent indicating a good dispersion at the nano scale of CNa in the matrix without apparent formation of aggregates. However, bionanocomposites with C10A were more opaque decreasing transparency with nanoclay addition. It indicates the formation of C10A clay aggregates in the matrix that scatter of light reducing the transparency of the samples. An intermediate transparency showed the bionanocomposites with C30B, suggesting an intermediate dispersion to that obtained with the other two nanoclays.

In order to a better evaluation of the dispersionstate of the different nanoclays into the TPS matrix, elemental mapping of fracture surfaces for the bionanocomposites was carried out by scanning electron microscopy coupled with energy dispersive X-ray (SEM–EDX). MMT nanoclays are mainly composed of silica and alumina. Figure 1 shows the silicon distribution maps on the fracture surface of the different TPS/MMT bionanocomposites.

The dispersion of nanoclays can be evaluated from the distribution of the light spots (silicon) through the TPS matrix. It can be seen that the dispersion of the nanoclay in the matrix depended on the type of nanoclay. Thus, natural CNa showed good and uniform dispersion in the matrix TPS for any of the three compositions studied. The organomodified C30B also exhibited a good dispersion, although some aggregates could be seen at the highest clay load. However,

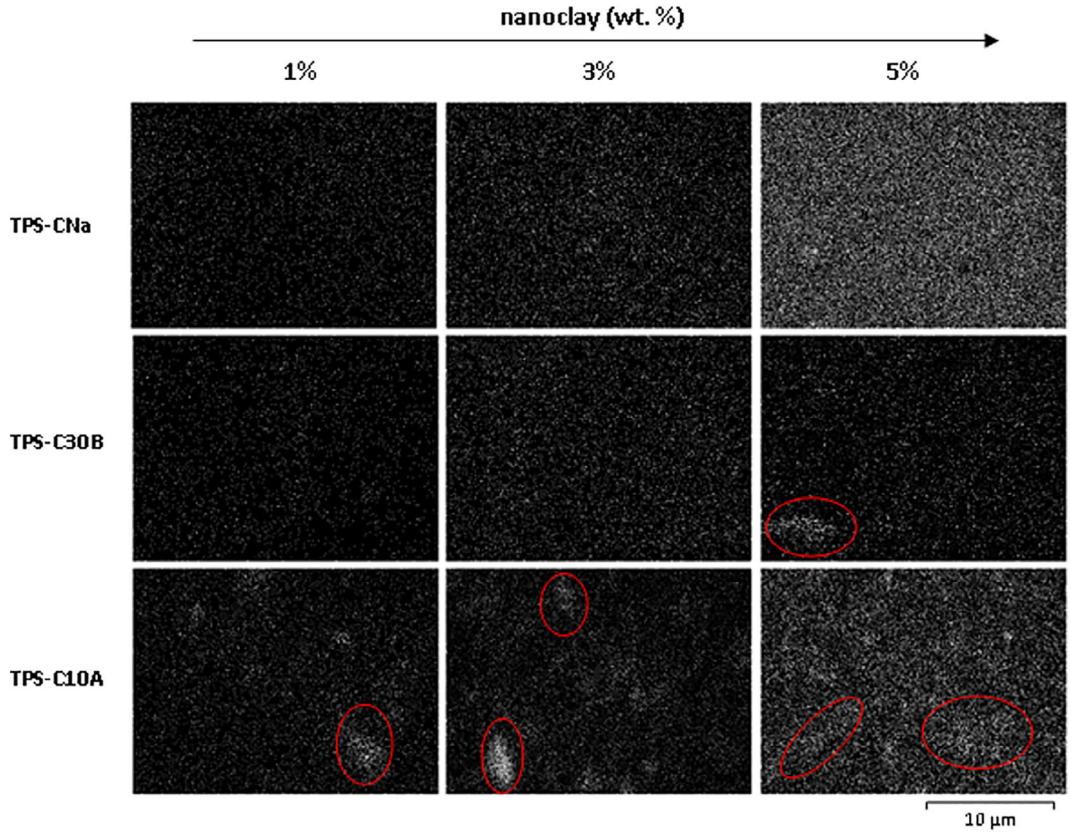

FIGURE 1 SEM/EDX micrographs of elemental silicon distribution (light spots) for the TPS/MMT bionanocomposites. Circles highlight some aggregates formed

when the organomodified C10A clay was used numerous aggregates were observed in all compositions.

A more detailed study of the dispersion state and the structure of the different TPS/MMT bionanocomposites was carried out by X-ray diffraction (XRD). Figure 2 shows the diffractograms in the range of $2\theta = 2°–10°$ of TPS/MMT bionanocomposites with the three nanoclaytypes compared tothe respective pure nanoclay. The position of the clay diffraction peak, 2θ, is indicated for each material. From the diffraction peak position, the clay interlayer spacing (d_{001}) was calculated. d_{001} values obtained for each bionanocomposite are listed in Table 2 and for each pure nanoclay in Table 1. The clay diffraction peak forthe bionanocomposites with 1 wt.% of nanoclay could not be clearly established, probably due to the low clay concentration, and therefore d_{001} values were not calculated either.

XRD is a classic technique to examine the state of intercalation/exfoliation of nanoclay in a thermoplastic matrix by analyzing the variation in the interlayer spacing of the clay when it is added to the matrix. It is desired that during melt processing the TPS molecules penetrate into the nanoclay gallery, forcing the platelets to separate and increasing d_{001}.[21] An increase in d_{001} results in a shift of the clay diffraction peak to lower angles. In theory, the diffraction peak should (1) be moved to lower 2θ values for intercalated structuresof the matrix into the clay layer galleries, (2) disappear completely for the exfoliated structures of the clay and (3) remain in the same position for phase separated structures.[19,26]

According to this, Figure 2 shows that the dispersion and the resulting structure of TPS/MMT bionanocomposites varied with the nanoclay type used. Thus, natural CNa nanoclay (Figure 2(A)) showed a XRD pattern with an intense peak at $2\theta = 7.15°$ corresponding to a d_{001} of 1.23 nm. In the TPS/CNa bionanocomposites, the CNa diffraction peak was moved at lower angles, $2\theta \approx 4.8°$, regardless the clay content resulting in an increase in the interlayer spacing ($d_{001} = 1.85$ nm). These results indicate an intercalated structure for TPS/CNa bionanocomposites where starch chains or glycerol molecules enter into the silicate layers increasing the clay gallery spacing but without reaching complete exfoliation. Similar results were found in the literature for TPS/CNa and attributed to the intercalation of glycerol molecules rather than starch chains.[27,28] Other authors, however, think that the similar size of glycerol and glucose units in starch makes it difficult to assess, on the basis of the change in the interlayer spacing, which component is the one that enters into the clay galleries.[25] It is worth noting that there is an apparent absence of the clay diffraction peak for the TPS/CNa bionanocomposite with 1% CNa, which suggests some exfoliation of the CNa platelets into the TPS matrix.

Organomodified C30B clay (Figure 2(B)) showed the main diffraction peak at $2\theta = 4.78°$ corresponding to a d_{001} spacing of 1.85 nm.

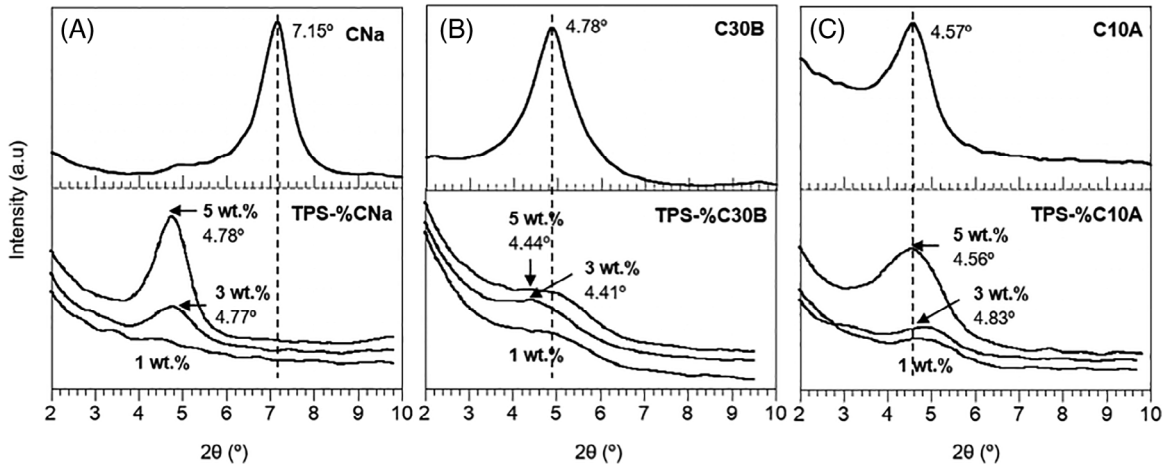

FIGURE 2 XRD patterns of TPS/MMT bionanocomposites compared with pure nanoclay for CNa (A), C30B (B) and C10A (C) nanoclays. The position of the diffraction peak of the nanoclay is indicated for each material

This peak was shifted slightly at lower angles in the TPS/C30B bionanocomposites, indicating only a small increase in its interlayer spacing. These results also suggest intercalated structures for the TPS/C30B bionanocomposites but with less intercalation than in the case of TPS/CNa bionanocomposites. Although the diffraction peak of the TPS/C30B bionanocomposites was slightly displaced, it was poorly defined, wide and with low intensity. This could indicate some exfoliation of small amounts of C30B in the TPS matrix for the TPS/C30B bionanocomposites.[29]

Finally, organomodified C10A (Figure 2(C)) showed a diffraction peak at $2\theta = 4.57^{\circ}$ corresponding to a d_{001} of 1.93 nm. Although the larger interlayer spacing of this clay could facilitate starch molecular intercalation, the diffraction peak of C10A remained in the same position for the bionanocomposites. Consequently, the interlayer spacing did not increase and no intercalation took place indicating the formation of phase separatedfor TPS/C10A bionanocomposites.

The results obtained by visual transparency, SEM/EDX, and XRD coincide in that the dispersion state of the nanoclay into TPS matrix was better for the natural CNa, followed by the organomodified C30B, while the worst dispersion was obtained with the organomodified C10A. These results suggest that the determinant factor for the dispersion and formation of intercalated/exfoliated nanocomposite is a good compatibility and interaction between the TPS matrix and the nanoclay, which occurs when the surface polarities are similar. It is important to note that starch is highly hydrophilic and the surface hydrophylicity of MMT clays follows the order CNa > C30B > C10A. The organomodified clayshave the advantage of a greater interlayer spacing, which could facilitate starch molecular intercalation,[8] however their hydrophobic nature makes them more ineffective in composing polar and hydrophilic biomacromolecules as starch.

C10A clay with dimethyl benzyl hydrogenated tallow quaternary ammonium cations is the most hydrophobic of the clays and the one that worst matches the polarity with the hydrophilic TPS. The lack of strong interactions between the ammonium cations of C10A and the TPS molecules disfavor the intercalation leading to the formation of phase separated with poor dispersion and presence of clay agglomerates.C30B clay is a more hydrophilic organoclay due to the hydroxyl groups present in the bis-2-hydroxyethyl quaternary ammonium cations. These hydroxyl groups can interact with the TPS molecules, favoring the penetration of TPS into the clay galleries and leading to the formation of intercalated structures with enough good dispersion. The best dispersion occurred with the natural CNa is possibly due to the strong interactions formed between the TPS molecules and CNa.[10] The hydroxyl groups of the starch are able to interact directly with the sodium ion of the clay gallery or with the edge hydroxyl groups of the clay layers, making a very compatible system.[16]

3.3 | Thermal stability

The effect of nanoclay addition on the thermal stability of TPS was evaluated by thermogravimetry (TG) where the weight loss of the sample was monitored as a function of temperature under an inert atmosphere. The TG curves and derivative thermogravimetric curves (DTG) obtained for neat TPS and TPS/MMT bionanocomposites with 5 wt.% of the three types of nanoclay are shown in Figure 3. The maximum decomposition temperature (T_{max}) was calculated from the peak of the DTG curve. Values of T_{max} and residue at 600°C obtained for each sample are listed in Table 3.

The weight loss during heating of neat TPS and TPS/MMT bionanocomposites mainly occurred in two steps. The first step occurred from room temperature to around 250°C and is associated to the loss by evaporation of low molecular weight molecules (water first and then glycerol). The other step of degradation took place in the range of 270°C to 400 °C and corresponds mainly to the thermal decomposition of starch by molecular dehydration with the final production of a carbonaceous residue.

The decomposition of starch began at approximately the same temperature in all materials, but slight variations occurred after this

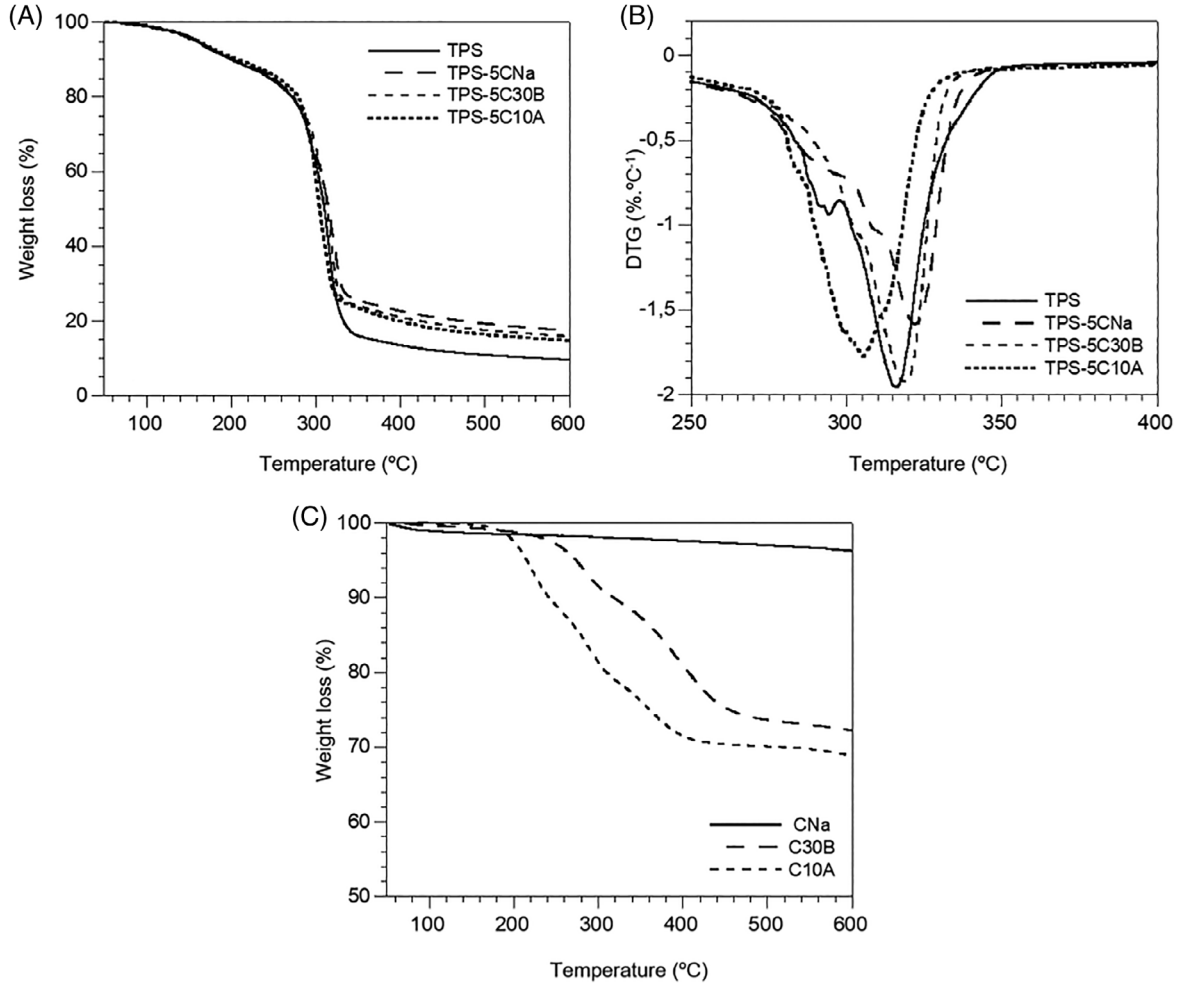

FIGURE 3 TG and DTG curves (A), (B) for neat TPS and TPS/MMT bionanocomposites with 5 wt.% of different MMT: CNa, C30B and C10A. TG curves (C) for CNa, C30B, and C10A nanoclays

TABLE 3 Thermal stability and dynamic mechanical properties for neat TPS and TPS/MMT bionanocomposites

	Thermal stability		Dynamic mechanical properties		
Sample	T_{max} (°C)	Residue at 600°C (%)	E' at 20°C (MPa)	$Tg_{glycerol}$ (°C)	Tg_{starch} (°C)
TPS	316.1	9.5	22.4	−49.2	5.0
TPS-1CNa	319.4	10.1	38.2	−48.3	5.3
TPS-3CNa	320.3	13.4	41.8	−47.6	6.1
TPS-5CNa	322.2	17.4	47.7	−46.5	6.4
TPS-1C30B	316.5	10.3	16.8	−49.4	3.5
TPS-3C30B	317.8	13.1	17.0	−49.5	4.5
TPS-5C30B	319.0	15.8	23.6	−48.8	6.2
TPS-1C10A	315.9	10.0	16.6	−49.4	3.1
TPS-3C10A	307.1	12.3	18.0	−50.0	2.7
TPS-5C10A	305.3	14.7	12.9	−51.7	−0.4

initial temperature depending on clay type. Thus, the maximum decomposition temperature (T_{max}), observed at 316.1°C for neat TPS, increased for TPS/C30B bionanocomposites and to a greater extent for TPS/CNa, however it decreased for TPS/C10A bionanocomposites. Therefore, the thermal stability of the TPS material improved by the addition of both natural CNa clay mainly and C30B organoclay, but it was deteriorated by the addition of C10A organoclay. This suggests that thermal stability depends on the

dispersion state of the nanoclay in the TPS matrix being improved for the intercalated nanocomposites. In intercalated structures, a labyrinth or tortuous pathstructure is formed in the matrix which could block or limit the diffusion of the gases and volatile products generated in the decomposition.[30]

These differences in thermal stability of bionanocomposites could be influenced by the early decomposition of the organic surfactants used in the organoclays, as can be seen from Figure 3(C) where TG curves of the pure nanoclays are shown. The nanoclays show a small initial degradation step corresponding to the water loss, which is more important to a higher hydrophilic character of the clay, that is, CNa > C30B > C10A. The organoclays show a second degradation step corresponding to the degradation of the organic alkyl ammonium surfactant that starts at about 190°C for C10A and at a higher temperature, about 250°C, for C30B. By contrast, natural CNa shows a great thermal stability in all the temperature range studied. This result is consistent with the thermal stability shown by the TPS/MMT bionanocomposites.

The residueof the materials increased with the addition of nanoclays and with the amount of the nanoclay added. The residue was higher for the bionanocomposites with natural CNa, that can be attributed to the high inorganiccontent of this nanoclay.

3.4 | Dynamic mechanical properties

DMA analysis has been carried out to check the effect of the nanoclay addition on the dynamo mechanical properties, that is, storage modulus and loss factor. Storage modulus (*E'*) is related to the elastic response of the material and it is a measure of its stiffness. *E'* values at room temperature (20°C) for TPS/MMT bionanocomposites and neat TPS are tabulated in Table 3.

It is observed that at room temperature the stiffness of neat TPS is improved by the incorporation of natural CNa, getting to double the *E'*value with a 5% of CNa. On the contrary, the incorporation of the organoclays (C30B and C10A) led to a decrease in the modulus and stiffness of neat TPS. By comparing both organoclays, the greatest decrease in material stiffness was obtained by adding 5% of the dispersed worst nanoclay, C10A; while the addition of 5% of C30B slightly exceeded *E'*value of neat TPS. These results indicate that for an efficient reinforcement of TPS with nanoclays it is crucial a favorable interaction and a homogeneous dispersion of the nanoclay in the TPS matrix as with CNa, which will facilitate the stress transfer from the matrix to the nanoclay, increasing the rigidity of the material.[10]

Tan δ curves as a function of temperature of TPS/MMT bionano composites and neat TPS for the three types of MMT nanoclays are shown in Figure 4.

All the materials showed two main relaxation peaks in Tan δ curves. It indicates partially miscible systems with two separated phases corresponding to starch-rich domains and glycerol-rich domains.[31,32] The relaxation located at lower temperatures, next to −50°C is associated with the glass transition of the phase rich in glycerol plasticizer,[33] while the broad relaxation occurred at higher temperatures corresponds to the glass transition of the starch-rich phase. The glass

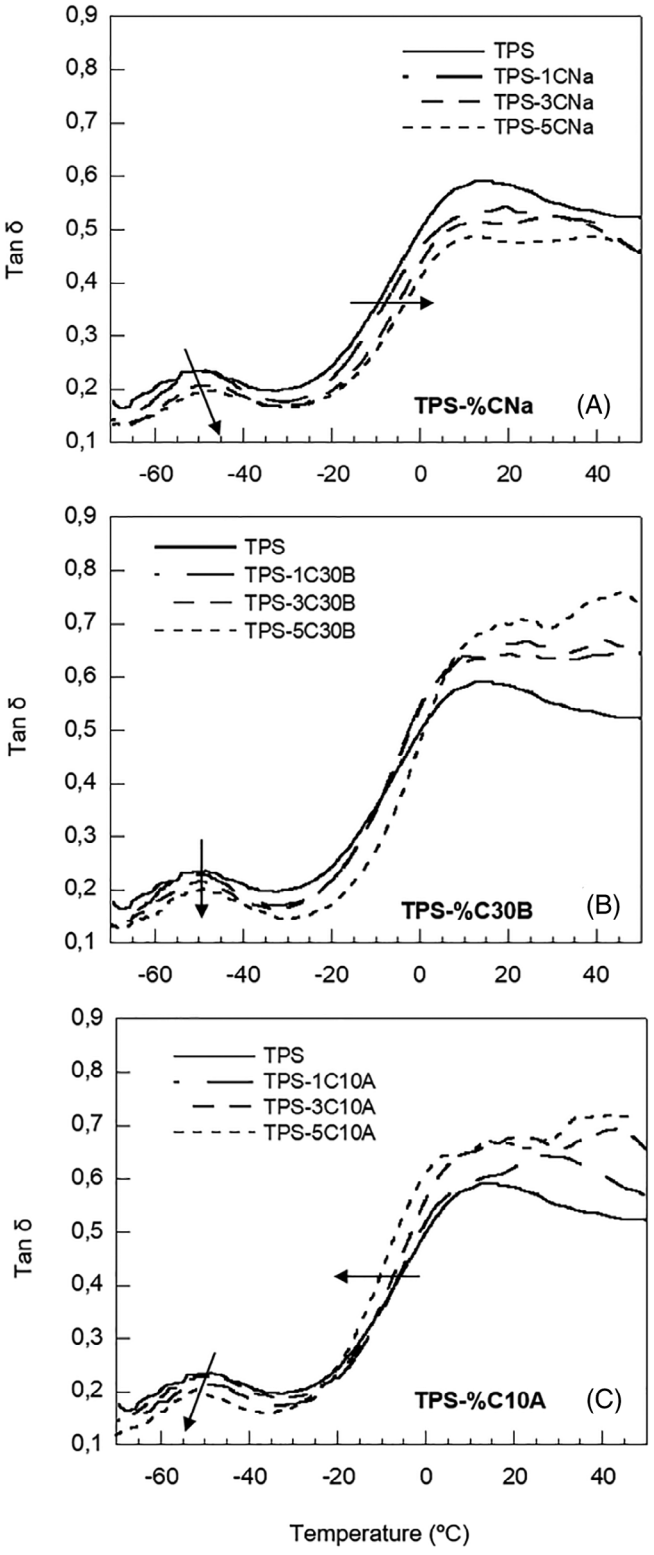

FIGURE 4 Tan δ curves of neat TPS and TPS/MMT bionanocomposites for different MMT: CNa (A), C30B (B) and C10A (C)

transition temperatures of both relaxations ($Tg_{glycerol}$ andTg_{starch}) were determined for neat TPS and TPS/MMT bionanocomposites and are listed in Table 3. $Tg_{glycerol}$ was determined at the maximum while Tg_{starch} was determined in the onset ofthe respective relaxations.

The relaxations of both phases were affected by the nanoclay addition in different ways depending on the type of MMT clay. Thus, when the most hydrophilic nanoclay (CNa) was added to TPS, the two glass transitions shifted to higher temperatures with the CNa content. It can be attributed, as was mentioned above, to the strong interactions and the good dispersion of CNa in the TPS matrix, which causes restriction in the mobility of the starch chains and glycerol molecules with the consequent increase in *Tg*. In contrast, for TPS/C10A bionanocomposites the two glass transitions shifted to lower temperatures compared to neat TPS, evidencing the poor interaction between the hydrophobic C10A clay and the hydrophilic TPS matrix. In TPS/C30B bionanocomposites, both relaxations remained practically at the same temperature than in neat TPS, which can be attributed to an intermediate compatibility between a more hydrophilic organoclay C30B and the hydrophilic TPS.

It is worth noting that the intensity in the relaxation of the starch-rich phase was increased with the incorporation of the two organomodified clays, however it was diminished by adding natural CNa. It indicates a more restricted mobility of the starch molecules in the presence of CNa clay but not with the organomodified clays.

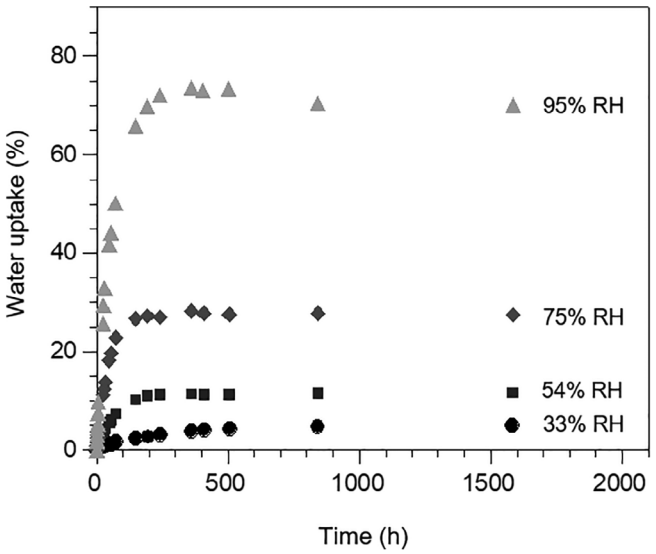

FIGURE 5 Water absorption-time curves for TPS-3CNa bionanocomposite under various relative humidity environments: 33% (●), 54% (■), 75% (♦) and 95% (▲)

3.5 | Water absorption

One of the main disadvantages of starch-based materials is their high water absorption capacity, as a result of their numerous hydroxyl groups which makes it highly hydrophilic and sensitive to water. Absorbed water acts as a plasticizer for starch increasing the mobility of the molecular chains and affecting the dimensional stability and properties of the TPS material.[25] Therefore, to increase the possibilities of industrial application any improvement in the water resistance of TPS materials is desired.

Water absorption isotherms (i.e., moisture content as a function of time) for TPS/MMT bionanocomposites and neat TPS were obtained at different relative humidities (RH): 33%, 54%, 75% and 95%, until the moisture content at equilibrium was reached. Figure 5 shows the absorption curves obtained at those RH for one of the bionanocomposites, TPS-3CNa, as an example. The rest of TPS/MMT bionanocomposites and neat TPS showed curves with similar trends. From water absorption curves, values of water uptake at equilibrium were determined for each material at the different RH and they are listed in Table 4.

The curves of water uptake showed an initial lineal region with rapid water absorption until about 100 h; and then the sorption rate was gradually decreased until finally a pseudo plateau region was reached indicating the water absorption equilibrium. At 95% RH, the curves of all the materials showed a slight mass loss after the maximum absorption. As was established in a previous work,[34] this mass loss must be attributed to the extraction of soluble material (mainly glycerol) provided by the liquid water deposited on the surface of the material and facilitated by the high content of absorbed water with around 70% at this high RH.

The RH of the environment was the most important parameter affecting water absorption of the TPS materials. As expected, the amount of water absorbed by the materials increased greatly with RH. Thus, the water absorbed by the materials was less than 6% and 12% in the environments of 33% RH and 54% RH respectively, while it exceeded 25% and 65% for 75% RH and 95% RH, respectively.

The incorporation of nanoclays in TPS caused only small changes in the water uptake at equilibrium, which were different depending on the environmental RH. Thus, by increasing the amount of any of the nanoclays in the sample, the water absorption of the material slightly decreased improving its water resistance, for all humidity environments except forthe highest RH (95%) where it was worsened. The water uptake at equilibrium is determined by the water sorption capacity of the material. The interactions between nanoclay and TPS cause a shielding and a reduction of the exposed OH groups of TPS in which the water molecules can be absorbed, thus decreasing the sensitivity to water for the TPS/MMT bionanocomposites.[10] However, at 95% RH the amount of water absorbed is so high (around 70%) that it could cause a weakening of the matrix-filler interface where water absorption is favored explaining the worsening in the water resistance at this high RH.

With respect to the effect of nanoclay type, the natural CNa proved to be the most effective clay to reduce water absorption in low and moderate humidity environments (33% RH and 54% RH). Conversely, in higher humidity environments (75% RH and 95% RH), the more hydrophobic clay, C10A, was the most effective or the least worsens the water resistance of the material. On the one hand and according to the above, the water resistance of material should improve with the most favorable matrix-filler interactions that follows the order, CNa > C30B > C10A, where the compatibility and the interfacial adhesion are greater. On the other hand, the water resistance of the material could also be affected by the hydrophilic character of the clay, so that the water resistance should decrease by increasing the hydrophilicity of the clay, where the water sorption capacity is greater, leading therefore to the opposite trend in water

TABLE 4 Water uptake at equilibrium and initial water absorption rate at various %RH for neat TPS and TPS/MMT bionanocomposites

	Water uptake at equilibrium (%)				Initial water absorption rate ($\%h^{-1}$)			
Sample	33% RH	54% RH	75% RH	95%RH	33% RH	54% RH	75% RH	95% RH
TPS	5.1	11.9	28.6	66.1	0.026	0.109	0.322	0.722
TPS-1CNa	5.0	11.7	28.4	68.6	0.024	0.105	0.319	0.713
TPS-3CNa	4.8	11.5	27.8	70.0	0.021	0.099	0.309	0.698
TPS-5CNa	4.5	11.2	27.4	71.8	0.018	0.095	0.303	0.688
TPS-1C30B	5.1	11.8	28.3	69.3	0.024	0.107	0.320	0.707
TPS-3C30B	4.9	11.6	27.8	70.6	0.023	0.105	0.315	0.691
TPS-5C30B	4.6	11.4	27.3	72.1	0.020	0.102	0.307	0.681
TPS-1C10A	5.1	11.8	28.1	67.2	0.025	0.108	0.321	0.708
TPS-3C10A	5.0	11.7	27.7	69.1	0.024	0.107	0.318	0.700
TPS-5C10A	4.9	11.5	27.2	70.2	0.023	0.106	0.310	0.682

resistance, that is, CNa < C30B < C10A. These opposite trends could explain the different behavior shown by TPS/MMT bionanocomposites depending on the environmental humidity. Thus, at high HR the samples have a high water content, which acts as a plasticizer giving mobility to the molecular chains and weakening the clay-matrix interactions. This could justify that the compatibility between the nanoclay and TPS matrix is a less important factor at high HR.

In addition to the water uptake at equilibrium, it is also important to evaluate the rate of the water absorption process. For that, the initial water absorption rate was determined for each TPS/MMT bionanocomposite and neat TPS, calculated as the average water absorption rate in the initial linear region. The obtained values are listed in Table 4. As Table 4 shows, TPS/MMT bionanocomposites had a slower initial water absorption rate than neat TPS, decreasing as the amount of nanoclay increases. The water absorption rate is determined by the diffusivity of the water molecules through the material. These results can be explained by the tortuous and thus longer effective pathway for the diffusion of water molecules created by the presence of clay platelets in the matrix.[35] A higher content of clay causes a greater obstructive action and consequently a longer pathway for the diffusion, slowing down the absorption process. On the other hand, the absorption rate should be affected bythe dispersion level of the nanoclay in the TPS matrix. It is expected that a better dispersion of the clay, which occurs with CNa > C30B > C10A, leads to more tortuous and longer diffusion pathway. This tendency was obtained at all humidity environments, except at 95% RH, where there was practically no difference with the type of clay.

4 | CONCLUSIONS

Bionanocomposites environmentally friendly based on wheat starch plasticized with glycerol and filled with three montmorillonite nanoclays were prepared by melt-processing. Three commercial MMT were examined: one natural Cloisite Na^+ (CNa), and two organomodified, Cloisite 30B (C30B) and Cloisite 10A (C10A). The effect of type and amount of nanoclay on processing properties, thermal stability, dynamic mechanical properties and water resistance of the materials was investigated.

The addition of any of the nanoclays increased the viscosity of the melt material during processing and improved the water resistance in all environments, except at very high relative humidity.

The dispersion of the nanoclays in TPS matrix improved with the hydrophilicity of the nanoclay, that is, CNa > C30B > C10A, attributed to the best polarity surface matching with the hydrophilic TPS. CNa was the most effective nanoclay to reinforce and improve the properties of TPS since it increased the thermal stability, stiffness and glass transition temperatures of neat TPS, as well as the resistance to water absorption especially in low and moderate humidity environments. In contrast, C10A was ineffective in reinforcing and an intermediate behavior was obtained for C30B, which improved thermal stability of neat TPS but it practically did not affect its dynamic mechanical properties.

In summary, the use of highly hydrophilic nanoclays that lead to bionanocomposites with good dispersion and strong matrix-clay interaction is an effective approach to reduce the drawbacks of starch-based materials This work sheds light on still unknown aspects of the behavior of TPS/MMT bionanocomposites depending on the type of MMT that are important for its use in different industrial applications such as food packaging.

ACKNOWLEDGMENTS

The authors would like to thank Xunta de Galicia Government and FEDER: program of consolidation and structuring competitive research units (ED-431C 2019/17) for financial support and ROQUETTE for kindly supplying wheat starch. 'Funding for open access charge: Universidade da Coruña/CISUG'

DATA AVAILABILITY STATEMENT

Data available in article supplementary material and on request from the authors

ORCID

Maite Rico https://orcid.org/0000-0003-1547-4914

REFERENCES

1. Esposito Corcione C, Striani R, Ferrari F, Visconti P, Rizzo D, Greco A. An innovative method for the recycling of waste carbohydrate-based flours. *Polymers*. 2020;12:1414.
2. Castaño J, Bouza R, Rodríguez-Llamazares S, Carrasco C, Vinicius RVB. Processing and characterization of starch-based materials from pehuén seeds (*Araucaria araucana* [Mol] K. Koch). *Carbohydr Polym*. 2012;88:299-307.
3. Area MR, Montero B, Rico M, Barral L, Bouza R, López J. Properties and behavior under environmental factors of isosorbide-plasticized starch reinforced with microcrystalline cellulose biocomposites. *Int J Biol Macromol*. 2020;164:2028-2037.
4. Giuri A, Colella S, Listorti A, Rizzo A, Esposito Corcione C. Biodegradable extruded thermoplastic maize starch for outdoor applications. *J Therm Anal Calorim*. 2018;134:549-558.
5. Stasi E, Giuri A, Ferrari F, et al. Biodegradable carbon-based ashes/maize starch composite films for agricultural applications. *Polymers*. 2020;12:524.
6. González K, Retegi A, González A, Eceiza A, Gabilondo N. Starch and cellulose nanocrystals together into thermoplastic starch bionanocomposites. *Carbohydr Polym*. 2015;117:83-90.
7. Montero B, Rico M, Rodríguez-Llamazares S, Barral L, Bouza R. Effect of nanocellulose as a filler on biodegradable thermoplastic starch films from tuber, cereal and legume. *Carbohydr Polym*. 2017;157:1094-1104.
8. Chivrac F, Pollet E, Avérous L. Progress in nano-biocomposites based on polysaccharides and nanoclays. *Mater Sci Eng R*. 2009;67:1-17.
9. Chivrac F, Angellier-Coussy H, Guillard V, Pollet E, Avérous L. How does water diffuse in starch/montmorillonite nano-biocompositematerials? *Carbohydr Polym*. 2010;82:128-135.
10. Xie F, Pollet E, Halley PJ, Avérous L. Starch-based nano-biocomposites. *Prog Polym Sci*. 2013;38:1590-1628.
11. Chivrac F, Pollet E, Schmutz M, Avérous L. New approach to elaborate exfoliated starch-based Nanobiocomposites. *Biomacromolecules*. 2008;9:896-900.
12. Díez J, Barral L, Bellas R, López J, Ramírez C, Rodríguez A. Exfoliated/intercalated silicate/hot styrene butadiene rubber nanocomposites: structure–properties relationship. *J Appl Polym Sci*. 2012;125:E705-E713.
13. Liu J, Tao Y, Zhou K, et al. The influence of typical layered inorganic compounds on the improved thermal stability and fire resistance properties of polystyrene nanocomposites. *Polym Compos*. 2017;38:E320-E330.
14. Lv Y, Chen J, Xu W, Kong M. Multiscale analysis on multiextrudedpoly(lactic acid)/organoclay nanocomposites: insights into the underlyingmechanisms of thermomechanical degradation. *Polym Adv Technol*. 2020;31:2742-2751.
15. Pirsa S, Sani IK, Khodaeivandi S. Design and fabrication of starch-nano clay composite filmsloaded with methyl orange and bromocresol green for determinationof spoilage in milk package. *Polym Adv Technol*. 2018;29:2750-2758.
16. Oleyaei SA, Almasi H, Ghanbarzadesh B, Moayedi AA. Synergistic reinforcing effect of TiO_2 and montmorillonite on potato starch nanocomposite films: thermal, mechanical and barrier properties. *Carbohydr Polym*. 2016;152:253-262.
17. Bittmann B, Bouza R, Barral L, Bellas R, Cid A. Effect of environmental factors on poly(3-hydroxybutyrate-co-3-hydroxyvalerate)/poly(butylene adipate-co-terephthalate)/montmorillonite nanocomposites with antimicrobial agents. *Polym Compos*. 2018;39:915-923.
18. Mathew S, Snigdha S, Mathew J, Radhakrishnan EK. Poly(vinyl alcohol): montmorillonite: boiled rice water (starch) blend film reinforced with silver nanoparticles; characterization and antibacterial properties. *Appl Clay Sci*. 2018;161:464-473.
19. Zeppa C, Gouanve' F, Espuche E. Effect of a plasticizer on the structure of biodegradable starch/clay nanocomposites: thermal, water-sorption, and oxygen-barrier properties. *J Appl Polym Sci*. 2009;112:2044-2056.
20. Aouada FA, Mattoso LHC, Longo E. New strategies in the preparation of exfoliated thermoplastic starch–montmorillonite nanocomposites. *Ind Crop Prod*. 2011;34:1502-1508.
21. Müller CMO, Laurindo JB, Yamashita F. Composites of thermoplastic starch and nanoclays produced by extrusion and thermopressing. *Carbohydr Polym*. 2012;89:504-510.
22. Romero-Bastida CA, Bello-Pérez LA, Velazquez G, Alvarez-Ramirez J. Effect of the addition order and amylose content on mechanical, barrier and structural properties of films made with starch and montmorillonite. *Carbohydr Polym*. 2015;127:195-201.
23. Dennis HR, Hunter DL, Chang D, et al. Effect of melt processing conditions on the extent of exfoliation in organoclay-based nanocomposites. *Polymer*. 2001;42:9513-9522.
24. Qiao X, Jiang W, Sun K. Reinforced thermoplastic acetylated starch with layered silicates. *Starch*. 2005;57:581-586.
25. Müller P, Kapin E, Fekete E. Effects of preparation methods on the structure and mechanical properties of wet conditioned starch/montmorillonite nanocomposite films. *Carbohydr Polym*. 2014;113:569-576.
26. Müller CMO, Laurindo JB, Yamashita F. Effect of nanoclay incorporation method on mechanical and water vapor barrier properties of starch-based films. *Ind Crop Prod*. 2011;33:605-610.
27. Zhang QX, Yu ZZ, Xie XL, Naito K, Kagawa Y. Preparation and crystalline morphology of biodegradable starch/clay nanocomposites. *Polymer*. 2007;48:7193-7200.
28. Lara SC, Salcedo F. Gelatinization and retrogradation phenomena in starch/montmorillonite nanocomposites plasticized with different glycerol/water ratios. *Carbohydr Polym*. 2016;151:206-212.
29. Park HM, Lee WK, Park CY, Cho WJ, Ha CS. Environmentally friendly polymer hybrids. Part I mechanical, thermal, and barrier properties of thermoplastic starch/clay nanocomposites. *J Mater Sci*. 2003;38:909-915.
30. Wang X, Zhang X, Liu H, Wang N. Impact of pre-processing of montmorillonite on the properties of melt-extruded thermoplastic starch/montmorillonite nanocomposites. *Starch*. 2009;61:489-494.
31. Wilhelm HM, Sierakowski MR, Souza GP, Wypych F. Starch films reinforced with mineral clay. *Carbohydr Polym*. 2003;52:101-110.
32. Castillo L, López O, López C, et al. Thermoplastic starch films reinforced with talc nanoparticles. *Carbohydr Polym*. 2013;95:664-674.
33. Teixeira EM, Pasquini D, Curvelo AAS, Corradini E, Belgacem MN, Dufresne A. Cassava bagasse cellulose nanofibrils reinforced thermoplastic cassava starch. *Carbohydr Polym*. 2009;78:422-431.
34. Rico M, Rodríguez-Llamazares S, Barral L, Bouza R, Montero B. Processing and characterization of polyols plasticized-starch reinforced with microcrystalline cellulose. *Carbohydr Polym*. 2016;149:83-93.
35. Mondragón M, Mancilla JE, Rodríguez-González FJ. Nanocomposites from plasticized high-amylopectin, normal and high-amylose maize starches. *Polym Eng Sci*. 2008;48:1261-1267.

SUPPORTING INFORMATION

Additional supporting information may be found online in the Supporting Information section at the end of this article.

How to cite this article: Derungs I, Rico M, López J, Barral L, Montero B, Bouza R. Influence of the hydrophilicity of montmorillonite on structure and properties of thermoplastic wheat starch/montmorillonite bionanocomposites. *Polym Adv Technol*. 2021;32(11):4479-4489. https://doi.org/10.1002/pat.5450